Drivers of the Mixed Layer Salinity Variability in the Seasonal Ice Zone of the Arctic Ocean

Alexandre Supply, Camille Lique, Nicolas Kolodziejczyk, Claude Talandier

JGR Oceans

RESEARCH ARTICLE
10.1029/2025JC022438

Special Collection:
The Arctic: An AGU Joint Special Collection

Drivers of the Mixed Layer Salinity Variability in the Seasonal Ice Zone of the Arctic Ocean

Alexandre Supply[1], Camille Lique[1], Nicolas Kolodziejczyk[1], and Claude Talandier[1]

[1]University Brest, CNRS, IRD, Ifremer, Laboratoire d'Océanographie Physique et Spatiale (LOPS), IUEM, Brest, France

Abstract The Arctic seasonal ice zone experiences complex atmosphere-ocean-ice interactions, including an intensification of the seasonal sea ice freezing and melting fluxes. However, these processes are still not fully elucidated and are generally poorly represented in state-of-the-art climate models. In this study, we focus on the seasonal ice zone, using a regional ocean—sea ice model at high resolution to provide a comprehensive quantification of the mixed layer salinity budget. The seasonal variability of the mixed layer salinity is clearly amplified in the region characterized by a seasonal sea ice, and results largely from the well-known 1D vertical balance between the freshwater flux at the surface arising from sea ice melt and freezing processes, and vertical mixing and entrainment occurring at the base of the mixed layer. Over the Arctic shelves, our results reveal a contrasted dynamics from this 1-D balance, with significant contributions from (a) horizontal advection due to the shallow bathymetry and (b) freshwater from the river discharges. Overall, the largest amplitudes of the mixed layer processes are found within less than 100 km on each side of the sea ice edge. This highlights the need to better observe and understand the ocean-sea ice-atmosphere processes in the seasonal and marginal ice zones.

Plain Language Summary In the Arctic, the sea ice melt and freezing have a leading impact on the ocean surface dynamics, mainly in the regions that are seasonally ice-covered. Due to difficulty to observe the ocean in these regions where sea ice forms during winter and melts during summer, the processes associated with the surface ocean seasonal dynamics remain poorly known. In this study, we use a numerical model run at high resolution to examine the seasonal cycle of the ocean surface conditions in the Arctic seasonal ice zone. The surface salinity varies largely in response to sea ice melt (releasing freshwater to the surface) and freezing (associated with brine rejections), which are compensated by a deepening of the mixed layer entraining water sitting below. Regionally, horizontal currents can also play a significant role in this balance, notably by transporting the freshwater inputs from the rivers along the coast. Overall, there is an amplified seasonality of the mixed layer depth and salinity within 100 km of the sea ice edge, suggesting a need to better monitor and understand these hot spots of sea-ice-atmosphere interactions.

Key Points:

- In the Arctic Seasonal Ice Zone, mixed layer salinity is mainly driven by a 1D balance between sea ice freshwater flux and vertical mixing
- However, on the shelves, horizontal advection of freshwater from the river runoff significantly modulates the 1D balance
- The mixed layer processes are largely intensified within 100 km around the sea ice edge

Correspondence to:
C. Lique,
camille.lique@ifremer.fr

Citation:
Supply, A., Lique, C., Kolodziejczyk, N., & Talandier, C. (2025). Drivers of the mixed layer salinity variability in the seasonal ice zone of the Arctic Ocean. *Journal of Geophysical Research: Oceans*, *130*, e2025JC022438. https://doi.org/10.1029/2025JC022438

Received 31 JAN 2025
Accepted 4 AUG 2025

Author Contributions:
Conceptualization: Alexandre Supply, Camille Lique, Nicolas Kolodziejczyk
Formal analysis: Alexandre Supply, Camille Lique, Nicolas Kolodziejczyk, Claude Talandier
Funding acquisition: Alexandre Supply, Camille Lique, Nicolas Kolodziejczyk
Methodology: Alexandre Supply, Camille Lique, Nicolas Kolodziejczyk, Claude Talandier
Project administration: Camille Lique, Nicolas Kolodziejczyk
Resources: Alexandre Supply, Camille Lique, Claude Talandier
Supervision: Camille Lique, Nicolas Kolodziejczyk
Visualization: Alexandre Supply

1. Introduction

In the Arctic Ocean, the temporal and spatial variations in salinity determine the upper ocean density and stratification (Carmack, 2007; Stewart & Haine, 2016). Such a salinity-driven stratification is characteristic of the polar regions and is required for sea ice to form (Carmack, 2007). Another well-known characteristic of the Arctic region is indeed the presence of sea ice, which has drastically declined over the past decades in response to the on-going climate change. Since 2003, the Arctic Ocean has lost one third of its winter sea ice volume, due to the decrease in coverage and the thinning of the multiyear ice (Kacimi & Kwok, 2022; Kwok, 2018), so that the Arctic is entering a seasonal sea ice regime associated with intensified water cycle and sea ice melting and freezing phases (Haine & Martin, 2017; Kinnard et al., 2008). These changes are particularly pronounced over the Arctic shelves (Årthun et al., 2021; Stroeve & Notz, 2018). We anticipate that the changes in sea ice conditions primarily impact the seasonal cycle of the Arctic Ocean mixed layer salinity (MLS) that is largely driven by the seasonality of ocean-sea ice interactions.

Peralta-Ferriz and Woodgate (2015) have performed a comprehensive description of the Arctic Ocean mixed layer temporal and spatial variability using all available in situ measurements, describing how the successive phases of sea ice melt and freezing induce a strong variability in MLS and mixed layer depth (MLD). During spring and summer, sea ice melt induces a freshening and stratification of the surface layer, resulting in a shoaling of the mixed layer. During winter, brine rejection salinizes the surface layer, inducing convection and a deepening

Writing – original draft: Alexandre Supply, Camille Lique, Nicolas Kolodziejczyk
Writing – review & editing: Camille Lique, Nicolas Kolodziejczyk, Claude Talandier

of the mixed layer (Lemke & Manley, 1984; Toole et al., 2010). In addition to these typical seasonal variations, the Arctic MLD further exhibits a large spatial variability between regions. In winter for instance, MLD remains particularly shallow in the Beaufort Sea and Canadian Basin (around 30 m), while it is as deep as 170 m on average in the ice-free parts of the Barents Sea (Peralta-Ferriz & Woodgate, 2015).

Further, the interactions between the Arctic mixed layer and sea ice are largely both ways. Because of the peculiar Arctic stratification, heat can be stored within the mixed layer during the ice-free period (Stroeve et al., 2014) or just below the mixed layer, forming a near-surface temperature maximum that can potentially store heat throughout winter and modulate sea ice formation as heat is entrained again into the mixed layer (Jackson et al., 2012; Kawaguchi et al., 2014; Smith et al., 2018; Steele et al., 2011; Timmermans, 2015).

Although 1D vertical processes may explain the robust first order dynamical balance of the mixed layer close to the sea ice edge (SIE; Dewey et al., 2017), additional processes need to be considered to understand the full complexity of the mixed layer dynamics. This includes for instance lateral processes, such as meltwater advection or dense water flowing under lighter water, that may induce restratification from submesoscales to regional scales (Crews et al., 2022; Timmermans et al., 2012). Wind may also drive some spatial variations of the mixed layer properties by advecting the river plume through Ekman transport (Hudson et al., 2024; Macdonald et al., 1999; Mulligan & Perrie, 2019; Tarasenko et al., 2021). More generally, over the Eurasian shelves, numerous river plumes provide a large amount of freshwater, enhancing the mixed layer stratification and leading to important mixed layer variability (Janout et al., 2016).

The diversity of the processes driving the Arctic Ocean mixed layer variability is expected to be regionally and seasonally dependent. Nevertheless, a pan-Arctic quantification of the different processes influencing the MLS budget remain hardly feasible from sparse in situ observations and partial satellite coverage due to sea ice. Also, how these processes are dependent on the region, season and seasonal sea ice regime remains a puzzling question in the Arctic Basin. In this study, we analyze a simulation performed with a regional Arctic-North Atlantic high-resolution model to quantify the MLS budget and examine its spatial and seasonal variability. The simulation and methods are presented in Section 2. The temporal and spatial variability of the Arctic mixed layer properties are quantified in Section 3. A full seasonal MLS budget is estimated in Section 4, and then we focus on the different terms of the budget in the region close to the SIE in Section 5. Conclusions and discussions are given in Section 6.

2. Data and Methods

2.1. Model Configuration

Our analysis relies on a simulation performed with the regional Arctic-North Atlantic high-resolution model configuration named CREG12 (Canadian REGional, Dupont et al., 2015). It is based on the NEMO 3.6 (Madec & the NEMO System Team, 2016) and LIM 3.5 (Rousset et al., 2015) numerical models for the ocean and sea ice components, respectively. The configuration covers the Arctic Basin and part of the North Atlantic (down to 27°N). It has a high horizontal resolution (3–4 km) in the Arctic Ocean, meaning that baroclinic eddies are resolved everywhere in the Arctic except on the shallow shelves (Meneghello et al., 2021; Regan et al., 2020). There are 75 vertical levels. The vertical grid spacing is finer at the surface (1 m) and increases with depth, with 8 levels within the top 10 m of the water column. This fine vertical resolution contributes to accurately capturing the ocean-sea ice interactions resulting from the sea ice seasonality (brines rejected at the ocean surface as sea ice forms, and freshwater release as sea ice melts). A nonlinear equation of state is used to compute density (EOS80; Fofonoff & Millard, 1983), meaning that we consider here a practical salinity in units of pss. Parameterizations include a Laplacian mixing of temperature and salinity along isopycnals and a horizontal biharmonic viscosity. Vertical mixing is based on a turbulence closure scheme (TKE; Blanke & Delecluse, 1993), and its numerical implementation follows closely the description made by Allende et al. (2024) (their control simulation).

Initial conditions are taken from the World Ocean Atlas 2009 climatology for temperature and salinity while the ocean is at rest. The initial sea ice thickness and concentration are taken from a long global ORCA12 simulation performed by the Drakkar group (Tréguier et al., 2014). Along the lateral open boundaries, monthly mean conditions (comprising 3D velocities, temperature and salinity, and sea ice thickness and concentration) taken from the same ORCA12 simulation are applied. Through Bering Strait, the transports of volume, heat and freshwater closely resemble the observational estimates from Woodgate (2018). Regarding atmospheric forcing, we use the latest version of the Drakkar Forcing Set (DFS 5.2, which is an updated version of the forcing set

described in Brodeau et al., 2010). Inputs from the river and ice sheet runoff have been corrected to include the large and increasing contribution from Greenland (Hu et al., 2019).

The simulation used in this study covers the period from 1979 to 2015 and is described in further details in Talandier and Lique (2021). Extended evaluation of the ocean and sea ice conditions in the Arctic Basin can be found in Regan et al. (2020), Barton et al. (2022) and Van Straaten et al. (2025). Here we focus on the period after 1994 to allow for an initial spin up of the ocean and sea ice conditions. Our analysis is done based on the 5-day average outputs.

2.2. Mixed Layer Budget

Following Peralta-Ferriz and Woodgate (2015), we defined the MLD using a 0.1 kg.m^{-3} density threshold from the surface density. The MLS budget is diagnosed following Moisan and Niiler (1998), Kolodziejczyk and Gaillard (2013), and Pellichero et al. (2017) as:

$$\partial_t S = \frac{S\, F_{surf}}{\rho\, H} - \vec{u}.\nabla S + A_h \Delta^2 S + \kappa_z \partial_z S + \frac{\Delta S}{H}(\partial_t H + \nabla H.\overrightarrow{u_H} + w_H) \quad (1)$$

with H the MLD, S the salinity, ρ the potential density and $\vec{u}$ the horizontal velocity, all three averaged within the mixed layer, $\overrightarrow{u_H}$ and w_H the horizontal and vertical velocities at the base of the mixed layer, F_{surf} the total surface freshwater flux, A_h the coefficient of horizontal mixing (or diffusivity), ΔS is the vertical gradient of salinity at the base of the mixed layer (defined as the difference between the salinity at the base of the mixed layer and the salinity 15 m below the mixed layer; Ren et al., 2011; Pellichero et al., 2017), and κ_z the vertical eddy diffusivity for salinity.

In Equation 1, the left-hand term is the MLS tendency. The first right-hand term corresponds to the surface flux:

$$\frac{S\, F_{surf}}{\rho\, H} = \frac{S}{\rho\, H}(F_{ice.} + E - P + R) \quad (2)$$

meaning that F_{surf} is the sum of the flux induced by the melting and freezing of sea ice (F_{ice}), evaporation (E) minus precipitation (P, from both rain and snow), and the river runoff (R). The second and third right-hand terms in Equation 1 correspond to horizontal processes, namely horizontal advection within the mixed layer ($\vec{u}.\nabla S$) and horizontal diffusion ($A_h \Delta^2 S$). The last two right-hand terms correspond to vertical processes, namely vertical diffusion and entrainment. Entrainment is only considered when the entrainment velocity $w_e = (\partial_t H + \nabla H.u_H + w_H)$ is positive as an outgoing flow at the base of the mixed layer will not induce any change in MLS.

We estimate the MLS budget for each grid point of the model domain using the 5-day means. Note that the vertical processes are estimated as the residual of the other terms in Equation 1. Indeed, the variations in MLD occur on very short timescales, making it difficult to estimate these terms with a reasonable accuracy as soon as the model outputs are not saved at each timestep of the simulation (360s in our case). We further consider specifically four regions that represent the diversity of conditions encountered within the Arctic Ocean (Figure 1a).

3. Seasonal Variability in Sea-Ice Conditions, Mixed Layer Depth and Salinity

We start by computing the annual average duration of the ice-free period at each grid cell over 1994–2014 (Figure 1b). The Barents Sea is characterized by the strong influence of an inflow of warm Atlantic Water that prevents the formation of sea ice throughout the year (Årthun et al., 2012). On average, the seasonal ice zone (defined as the area partially covered by sea ice during the year) represents 60% of the Barents Sea surface while 28% is permanently ice free and only 12% of the surface is permanently ice covered. Overall, the spatial pattern of the sea ice conditions in the Barents Sea (Figures 2a–2d and 3) is coherent with observations and is likely driven by the influence of Atlantic Water and sea ice import in this area (Barton et al., 2022; Lind et al., 2018). Similarly, the Eurasian shelves and the Chukchi and Beaufort shelves are mainly occupied by the seasonal ice zone (64% and 73% respectively). In contrast, most of the deep basin is characterized by a perennial ice zone (92%), with a thicker ice all year long and a weak seasonal variability (Figures 2a–2d and 3).

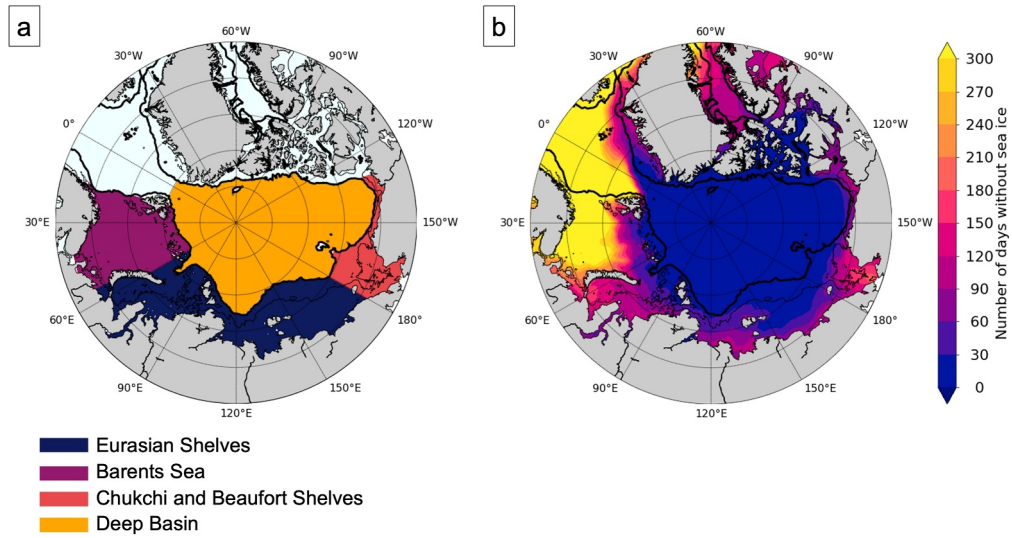

Figure 1. (a) Definitions of the four regions considered in this study; (b) Map of the annual average of the ice-free period between 1994 and 2014. The thick black line corresponds to isobath 500 m and the thin black line to isobath 50 m.

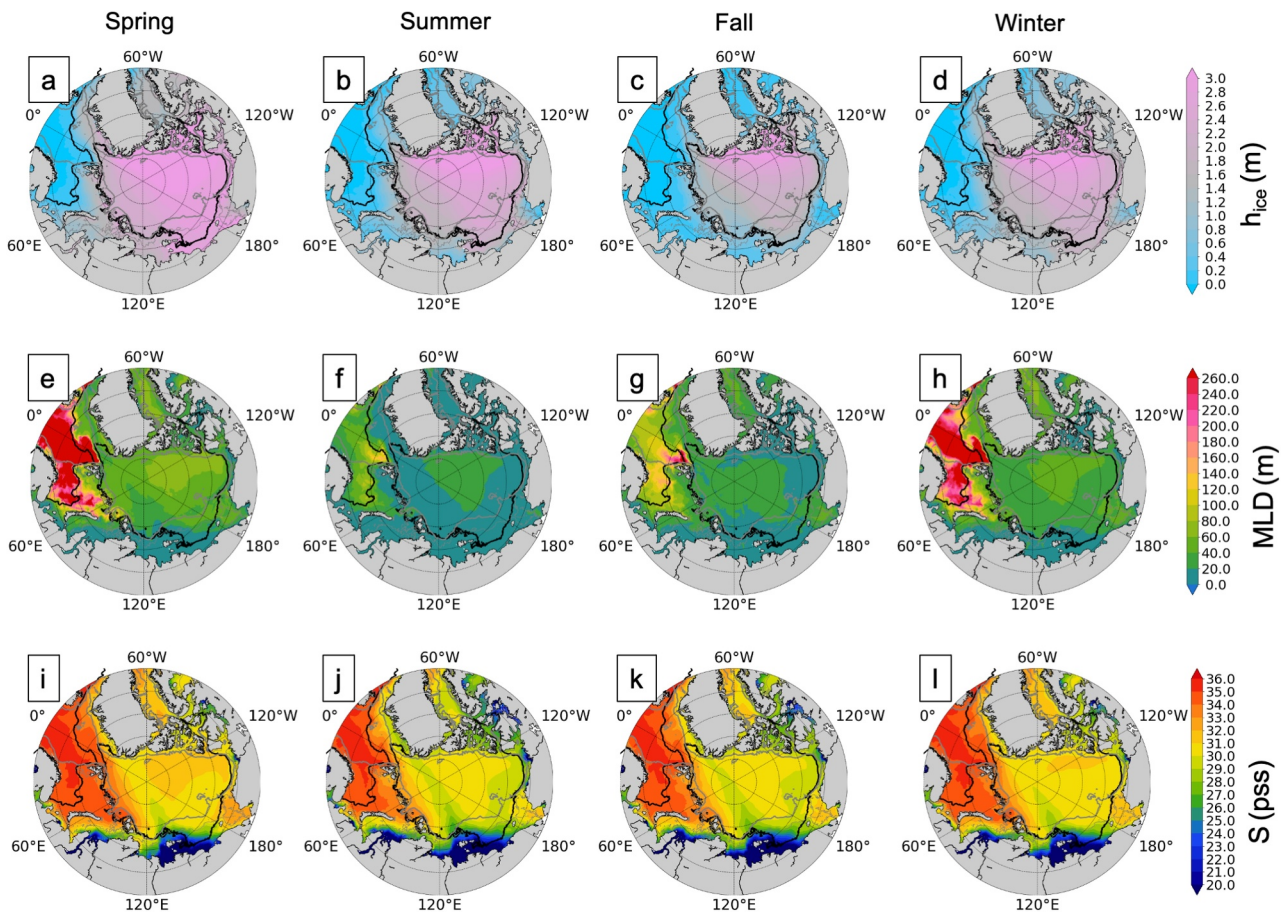

Figure 2. Maps of seasonal average (over the period 1994–2014) sea ice thickness (a–d), mixed layer depth (e–h) and mixed layer salinity (i, j) for spring (March, April, May—a, e, i), summer (June, July, August—b, f, j), fall (September, October, November—c, g, k) and winter (December, January, February—d, h, l). The black lines correspond to the transitions between the ice free zone, the seasonal ice zone and the perennial ice zone. The thick gray line corresponds to isobath 500 m and thin gray line to isobath 50 m.

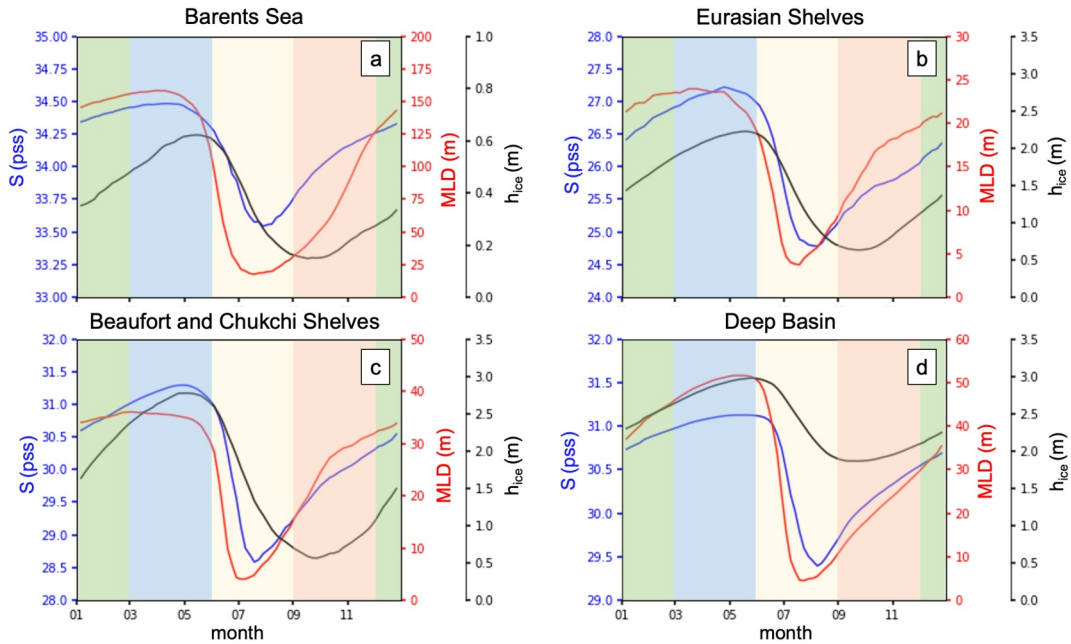

Figure 3. Average seasonal cycles (over the period 1994–2014) of sea ice thickness (black), mixed layer salinity (blue) and mixed layer depth (red) for the four regions shown in Figure 1a: the Barents Sea (a), the Eurasian Shelves (b), the Beaufort and Chukchi Shelves (c) and the Deep Basin (d). The change of background colors corresponds to the different seasons.

The Barents Sea exhibits the deepest MLD (more than 150 m on average in winter and spring; Figure 3), with deeper MLD in its ice-free parts (Figures 2e–2h), which is consistent with observations (Peralta-Ferriz & Woodgate, 2015). Over the Eurasian shelves and the Chukchi and Beaufort shelves, the MLD seasonal variability is limited by the shallow bathymetry and thus the MLD does not exceed 40 m (Figures 3b and 3c). In the deep basin, the MLD reaches deeper values on average than over the Eurasian shelves and the Chukchi and Beaufort shelves but remains shallower than in the Barents Sea (Figure 3d). Here again, the model MLDs are in close agreement with the observations reported by Peralta-Ferriz and Woodgate (2015), with a seasonal variability between 5 and 50 m.

We then examine the seasonal variations in MLS. Over the Arctic shelves, there are large spatial variations in MLS (Figures 2i–2l). In the Barents Sea, the MLS varies seasonally between 33.5 and 34.5 pss. It is characterized by the presence of a polar front between the Atlantic and Arctic waters (Lind et al., 2018), and the signature of the salty Atlantic Water inflow along the front close to the SIE (Oziel et al., 2016). The MLS in the Beaufort and Chukchi shelves is between 28.5 and 31.5 pss on average (Figure 3c), and is largely influenced by the advection of Pacific Water from the Bering Strait (Aksenov et al., 2016; Woodgate et al., 2012). In contrast, the MLS in the Beaufort and Eurasian shelves is fresher. These regions are under the influence of large river plumes that result in low MLS over large parts of the shelves (e.g., the Mackenzie in the Beaufort shelf, the Ob and the Yenisey in the Kara Sea and the Lena in the Laptev Sea). Over the Eurasian shelves, the average MLS varies between 24.8 and 27.2 pss (Figure 3b). The lowest MLS values are visible in the seasonal ice zone, which also corresponds to areas close from the coast, and thus under the influence of rivers runoff. In contrast to the shelves, the MLS in the deep basin exhibits smaller spatial and seasonal variability (varying between 29.5 and 31 pss over the year; Figure 3d), with higher MLS on the Eurasian side than on the Canadian Basin and the Beaufort Gyre.

Despite some regional differences, all the regions exhibit a similar timing of the seasonal variations of the different quantities considered here (Figure 3), that align well with the seasonal cycle obtained from observations by Peralta-Ferriz and Woodgate (2015) for these different quantities. During spring, MLS and sea ice thickness increase while the MLD reaches its maximum and starts to decrease at the end of the period. The summer period corresponds to a fast and strong decrease until July/August in MLD and MLS, while sea ice thickness continues to decrease to reach its minimum in September/October. During fall and winter, while sea ice thickness increases, MLS increases and the MLD deepening slows down.

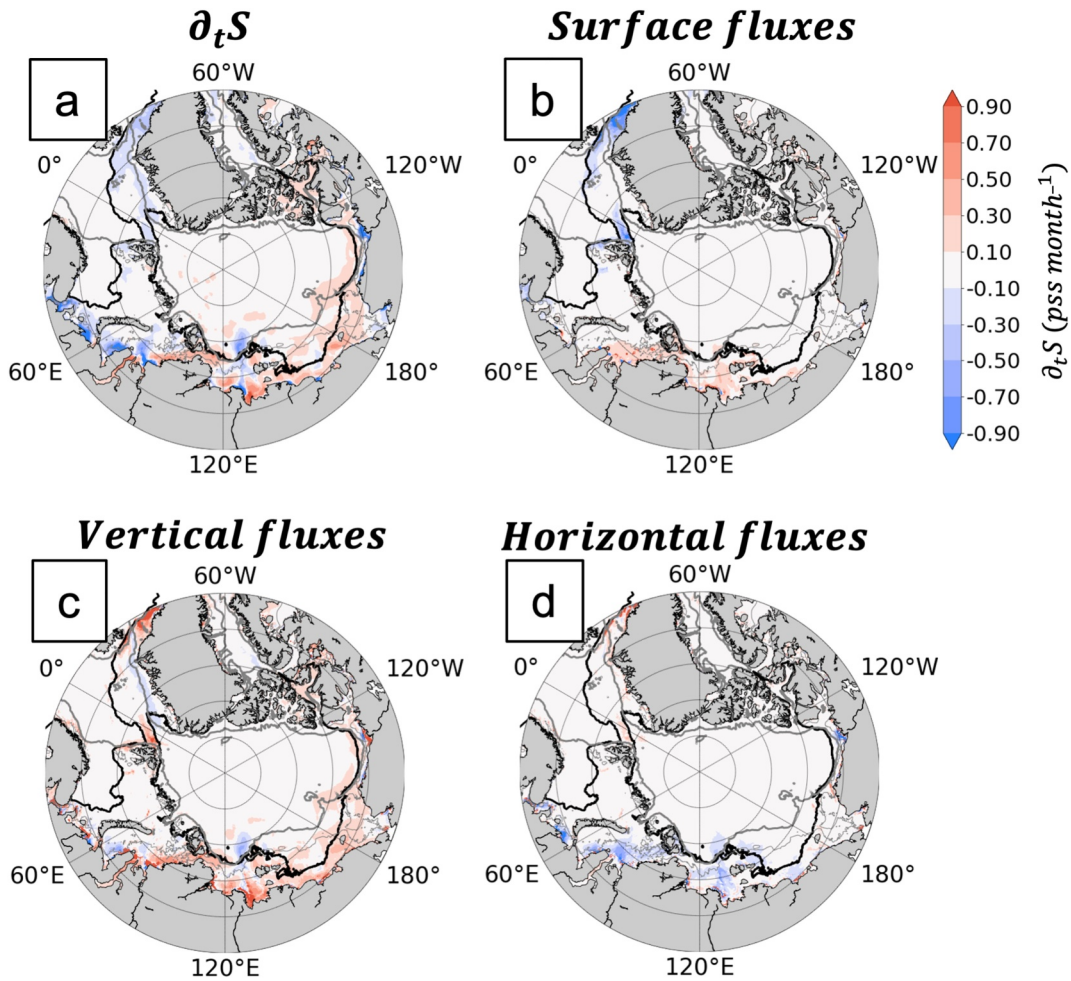

Figure 4. Maps of the different contributions to mixed layer salinity budget in spring: (a) salinity change ($\partial_t S$); (b) surface flux; (c) vertical flux; (d) horizontal flux. The black lines indicate the limits of the seasonal ice zone. The thick gray line corresponds to isobath 500 m and thin gray line to isobath 50 m.

4. Seasonal Budget of the Mixed Layer Salinity

We then estimate the full MLS budget from Equation 1. Results are shown as maps for each season (Figures 4–7) and as time series averaged over the four regions of interest (Figure 8).

During spring, the MLS tends to slightly increase on average, with the largest increase localized in the seasonal ice zone and over the shelves (Figures 4 and 8). This positive $\partial_t S$ results from the sea ice freezing and the vertical flux, associated with a deepening of the mixed layer. The largest salinity increase is visible in the vicinity of the river mouths in the Eurasian shelves and the Chukchi and Beaufort shelves, with values of $\partial_t S$ values between 0.1 pss month^{-1} and 0.3 pss month^{-1}. In contrast, the horizontal flux drives a negative $\partial_t S$ over most of the shelves. In addition to the overall positive $\partial_t S$, some negative spots of $\partial_t S$ are seen along the coasts of the Barents Sea and the Eurasian shelves (due to the advection of riverine water and negative vertical fluxes) and along the Greenland Shelf (due to sea ice melting and negative vertical fluxes). Some of these areas of negative $\partial_t S$ also exhibit a negative contribution from the vertical flux.

In summer, the main pattern is a decrease in MLS, with a value around −1 pss month^{-1} (Figure 5). This decrease in MLS arises from large surface and vertical fluxes that partly compensate each other. This is particularly true over the shelves, where the surface and vertical fluxes can locally exceed −3 pss month^{-1} and 2 pss month^{-1}, respectively (Figures 8b and 8c). The largest surface and vertical fluxes are found in the Kara and Chukchi seas,

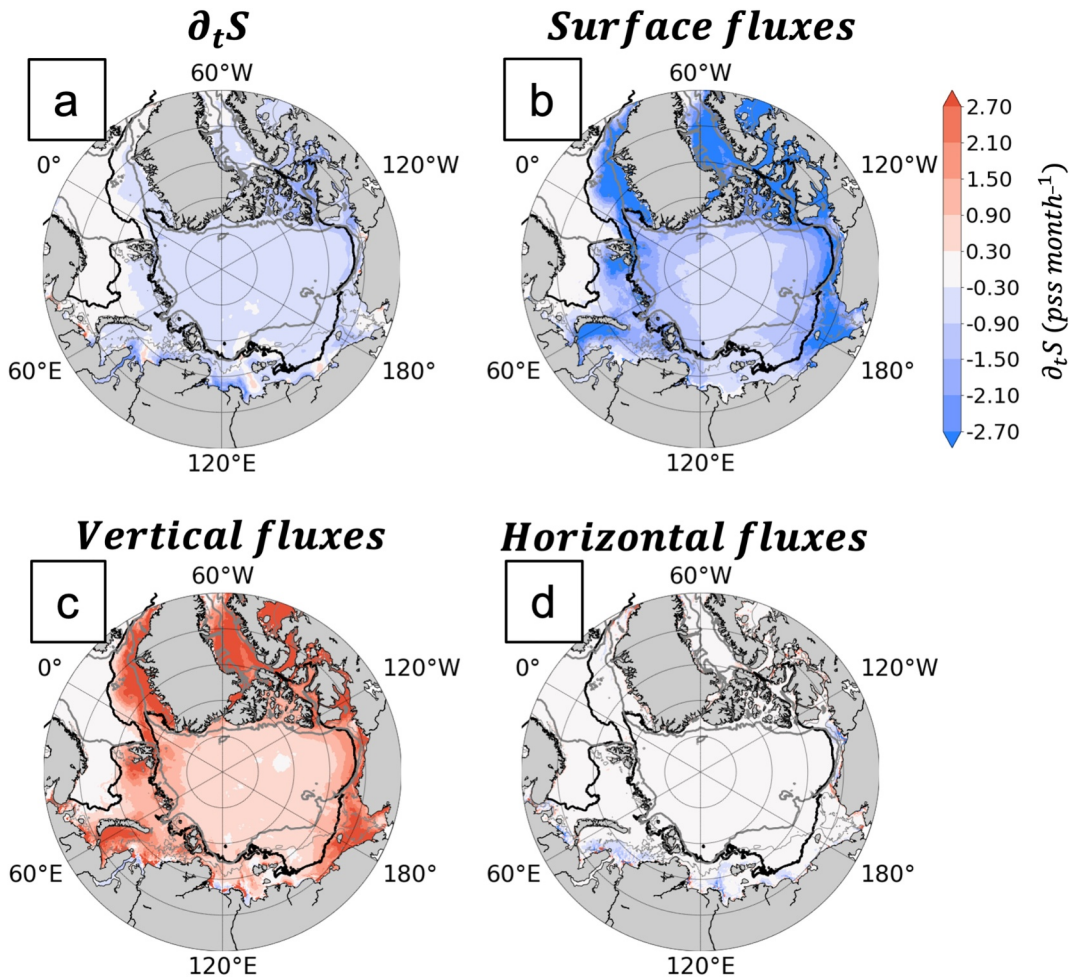

Figure 5. Same as Figure 4 but for summer. Note the different colorbar used here.

and over the Baffin Bay and the Greenland Shelf. Figure 8 also suggests that summer can indeed be divided into two phases, consistent with the different timing characterizing the MLD, MLS and sea ice thickness seasonal cycles (Figure 3): (a) a fast shoaling until July or mid-July, when the amplitude of the MLS change induced by the sea ice melting is larger than this due to the vertical flux, resulting in a negative $\partial_t S$; and (b) a slow deepening of the MLD associated with a MLS increase, when vertical mixing prevails over the impact of the sea ice melt, that continues until fall. For example, in the Chukchi and Beaufort seas, the average freshening first reaches its minimum of -2 pss month^{-1} and then increases again to roughly 0.6 pss month^{-1} for a few months.

During fall, sea ice melt halts and the MLS tends to increase, primarily because of the entrainment of saltier water from below the mixed layer (Figure 6). The contribution of the vertical flux strongly changes from the start to the end of fall. In the Eurasian shelves and the Beaufort and Chukchi shelves, this contribution decreases from approximately 1.2 pss month^{-1} to 0.3 pss month^{-1} (Figure 8). Over the Eurasian shelves, the surface flux, associated with brine rejection as sea ice forms, also contributes to the MLS increase in the vicinity of the river mouths, but this effect is largely counterbalanced by the negative contribution from the horizontal flux, due to advection of riverine waters. Near Fram Strait and in the Chukchi Sea, where sea ice tends to melt during this period, the MLS increase remains rather small. Over the Eurasian shelves, brine rejection induces the largest MLS increase. On average, the Chukchi and Beaufort shelves exhibit the largest MLS increase, with tendency close to 3 pss month^{-1} over large areas.

During winter, the main balance for the MLS budget is largely similar to the balance found for fall, with an increase in MLS caused by the vertical processes, although the values are overall weaker (around 0.2 pss month^{-1}), especially in the interior of the Arctic Basin (Figures 7 and 8). During this period, the relative

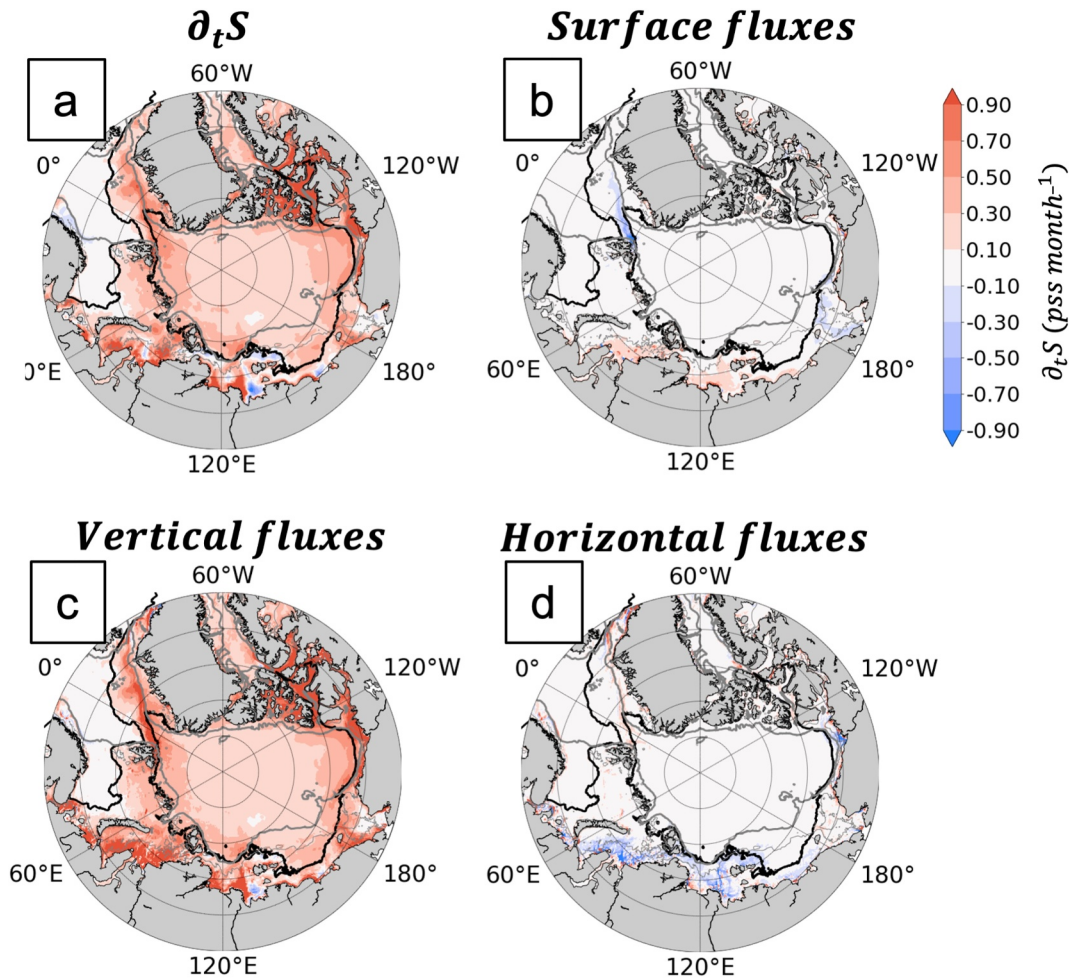

Figure 6. Same as Figure 4 but for fall.

impact of sea ice formation on MLS becomes stronger. The Eurasian shelves are a hotspot for the surface flux induced by sea ice freezing, but there the change in MLS is partly compensated by horizontal processes.

5. Mixed Layer Salinity Dynamics at the Sea Ice Edge

In this section, we focus on the MLS budget in the vicinity of the SIE, which is defined as the 15% sea ice concentration contour. To that aim, each grid point of the model output is characterized by its distance from the closest contour of 15% concentration. We then classify the grid point depending if the local concentration is higher or lower than 15% to know if the point is on the inner or outer side of the SIE. Figure 9 shows the MLS budget per season as a function of the distance from the SIE. During spring (Figure 9a), the vicinity of the SIE (50 km on both sides, with positive distances indicating ice-free areas and negative distances indicating ice-covered areas) is characterized by a decrease in MLS. There, the MLS change induced by both sea ice melt and river runoff fully explains the amplitude of $\partial_t S$, in spite of a strong and relatively persistent vertical flux that tends to oppose the freshening. Note that, at this early time of the melting season, river runoff plays a major role, contributing up to -0.5 pss month^{-1}. This is because at this time of the year, the SIE is still found close to the coast in many regions, and especially over the Eurasian shelves. Under sea ice, as the distance from the SIE increases, the sea ice melt contribution gradually reduces, while the horizontal fluxes contribution to the freshening increases in the first 100 km from the SIE and then remains roughly constant. During this period, the mixed layer is relatively deep (Figure 9e), with a deeper mixed layer found in the ice-free area (between 250 and 400 m on average) than under sea ice (between 100 and 200 m). One should keep in mind that this contrast is partly due to the fact that the ice-free regions during that period correspond to the regions that are ice-free all year long.

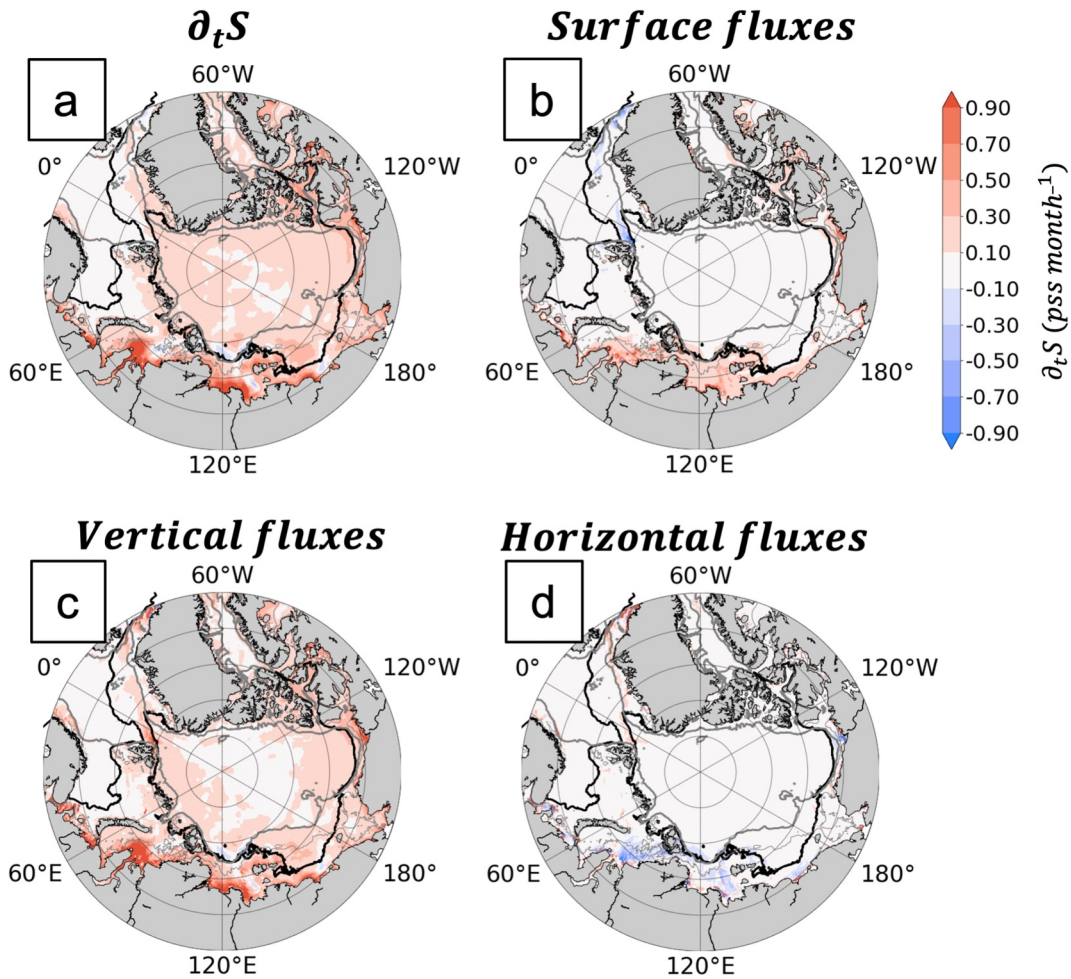

Figure 7. Same as Figure 4 but for winter.

During summer, the mixed layer is the shallowest (less than 30 m), especially at the SIE where it remains above 5 m (Figure 9b). These shallow mixed layers result from the large ice melt flux (up to −4 pss month^{-1}; Figure 9b) that tends to stratify the upper ocean layer. This makes the mixed layer particularly sensitive to changes induced by surface and vertical fluxes. Interestingly, $\partial_t S$ changes sign at the SIE: under sea ice, the mixed layer is getting fresher while in ice-free regions the mixed layer gets saltier. This is explained by the dominance of melting in the sea ice covered region while vertical mixing (between 1 and 5 pss month^{-1}) is dominant in the ice-free region, where the melt ceases as sea ice retreats. There, the mixed layer deepens, and the MLS increases as the distance from the SIE increases, in response to the contribution from the vertical flux (Figure 9b). Once again, the strongest flux is visible within ±50 km from the moving SIE. During summer, the contribution from the horizontal flux is stronger in the ice-free area, offsetting the contribution from the river runoff and thus resulting in a MLS increase.

During fall, $\partial_t S$ is positive everywhere, in response to the sea ice freezing onset (Figure 9c). Also, the amplitudes of the $\partial_t S$ absolute values are twice smaller than during summer (less than 0.5 pss month^{-1} vs. more than 1 pss month^{-1} on both sides of the SIE in summer). On both sides of the SIE, the contribution from the vertical flux is the main driver of the salinity increase and is again intensified closer to the SIE. In the sea ice free region, the horizontal advection (likely of freshwater from river runoff) induces a negative $\partial_t S$ on both sides of the SIE, albeit with a smaller amplitude.

Last, in winter, MLS and MLD increase close to SIE (Figures 9d and 9e). The mixed layer reaches its deepest annual value and exceeds 100 m under sea ice and 400 m in the ice-free region. The average is largely dominated by the deep MLD found in the ice-free Barents Sea during winter. $\partial_t S$ is mainly explained by the contributions

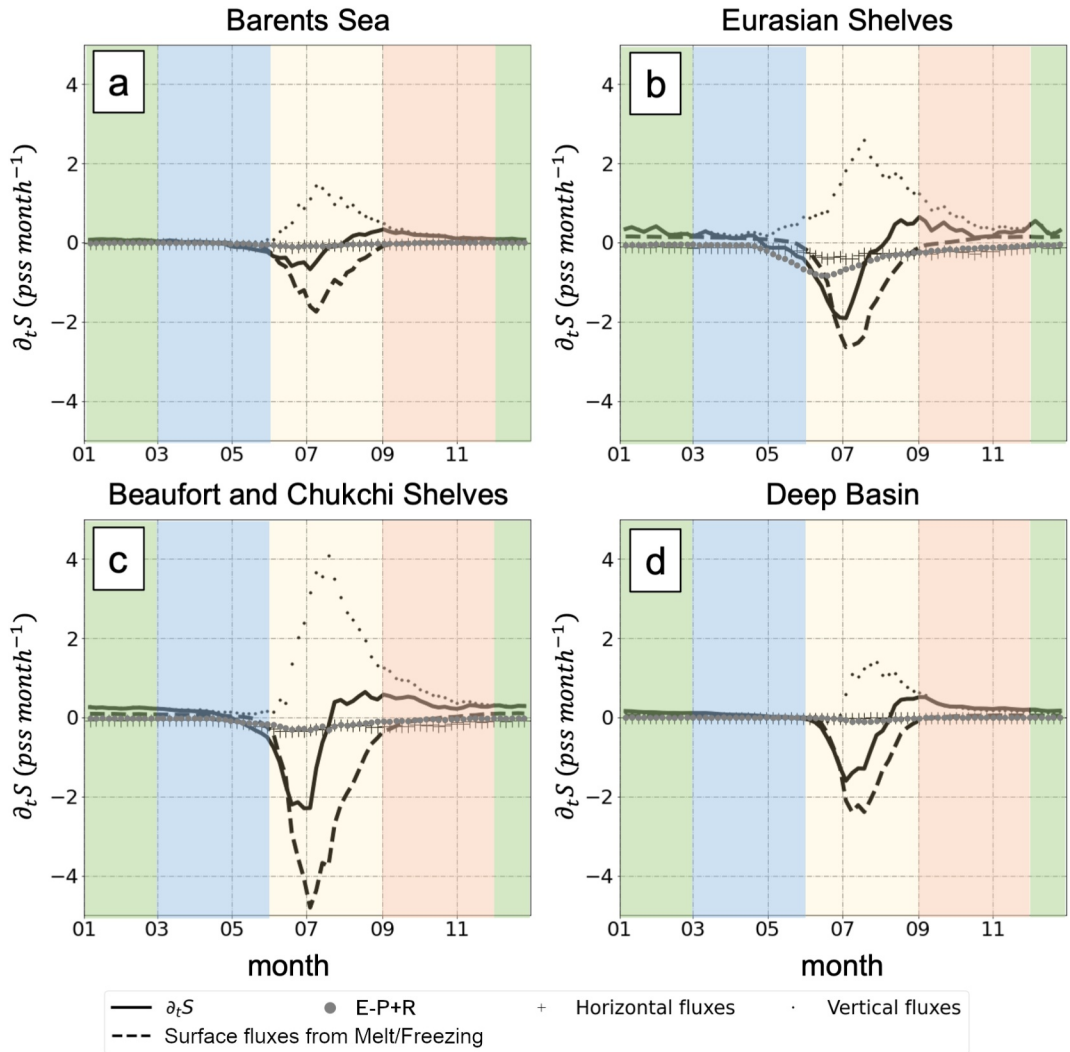

Figure 8. Average seasonal cycles (over the period 1994–2014) of the mixed layer salinity budget for the four regions shown in Figure 1a: the Barents Sea (a), the Eurasian shelves (b), the Beaufort and Chukchi shelves (c) and the deep basin (d). The change of background colors corresponds to the different seasons.

from freezing (under sea ice) and the vertical flux, although its amplitude is lower than during the other seasons (reaching only 0.1 pss month^{-1} at more than 150 km of the SIE under the sea ice).

6. Discussion and Conclusion

The Arctic Ocean is characterized by an expanding seasonal ice zone, where the large seasonal variations of the sea ice conditions influence the seasonal variability of the mixed layer, and in particular its salinity. Based on the detailed quantification of a salinity budget in the mixed layer applied to the outputs of a high-resolution ocean-sea ice model, we have shown that, on average, there is a seasonal balance between the contributions to the change in mixed layer salinity of sea ice freezing/melting and the vertical flux at the base of the Arctic Ocean mixed layer. It is interesting to note that, although the amounts of freshwater brought to the ocean surface by sea ice freezing and melting are roughly of equal amplitudes (53×10^5 m^3/s and -58×10^5 m^3/s on average over 1994–2014, respectively), their impacts on the mixed layer salinity are fundamentally asymmetric over a seasonal cycle. Indeed, the melt-induced freshwater flux, which is large during a short period of time in summer, tends to create a thin stratified upper layer. In contrast, the negative flux from sea ice brine rejection is smaller but sustained over a longer period, when the mixed layer is also deeper. Vertical processes (mixing and entrainment) also play a

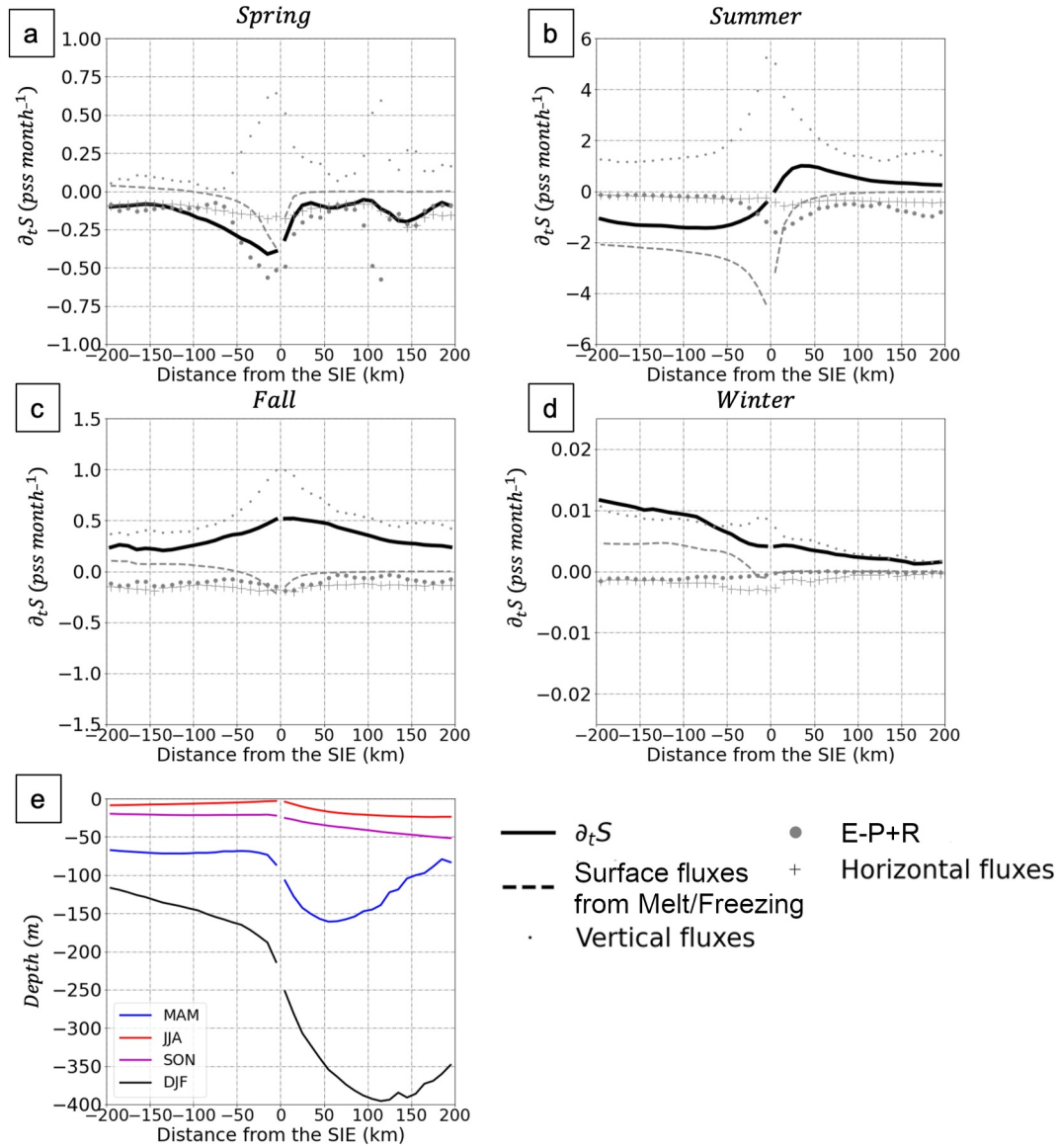

Figure 9. Mean seasonal mixed layer salinity budget as a function of distance from the sea ice edge (SIE) during spring (a), summer (b), fall (c), and winter (d). Mean seasonal spatial variations of the mixed layer depth as a function of distance from the sea ice edge (e). Positive distances from the sea ice edge correspond to ice-free areas and negative distances correspond to ice-covered areas.

different role depending on the season and region considered. In regions where sea ice retreats, the vertical mixing tends to respond to the surface freshening to destroy the vertical haline gradient at the base of the mixed layer. In contrast, during winter, the vertical processes result from brine rejection under the ice and deep convection in the ice-free region of the Barents Sea. Over the shelves, advection and river runoff also significantly contribute to spatially redistributing freshwater in the mixed layer. Despite their different dynamical regimes and forcing by the sea ice and atmospheric conditions, and inflow from the remote regions, the different parts of the deep basin (namely the Canadian and Eurasian basins) appear to be characterized by a similar mixed layer salinity budget. This similarity may arise from the fact that we only consider the mean seasonal cycle over 1995–2014, when both basins were largely ice-covered all year long, and the similarity could thus not continue in the future.

A striking result of our study is that the mixed layer salinity change and flux are generally largely intensified within 50 km of the sea ice edge (defined here as the 15% sea ice concentration contour), making the sea ice edge a hot spot for the seasonal variability. There, the sea-ice induced surface freshwater fluxes are intensified and

largely counterbalanced by strong vertical oceanic processes (similar to what was observed by Dewey et al., 2017 in the Canadian Basin). In addition, we also found that over the shelves and in the region characterized by large river plumes, horizontal fluxes of fresher water more strongly impact mixed layer salinity budget close to the sea ice edge, affecting the whole mixed layer salinity budget at the scale of the shelves.

Although our mixed layer salinity budget suggests that the lateral fluxes within the mixed layer is not the main driver of the variations of the mixed layer salinity, advection is most likely playing a large role in setting the stratification, which then modulates the evolution of the mixed layer depth (Peralta-Ferriz & Woodgate, 2015) and the properties of the water masses potentially entrained in the mixed layer. For instance, recent changes of the Atlantic Water inflow through Fram Strait and the Barents Sea have induced a weakening of the stratification in parts of the Eurasian Basin (Polyakov et al., 2020). In our framework, such a change would have a signature in the terms accounting for the vertical processes within the mixed layer.

Last, we acknowledge that our model, with its typical 3–4 km resolution, may not capture some of the small-scale processes that could be important for the evolution of the mixed layer and its salinity. For instance, it does not fully resolve the sea ice heterogeneity in the MIZ, or the submesoscale processes (O(1 km)), which may be important close to the sea ice edge (Manucharyan & Thompson, 2017) and locally affect the mixed layer salinity budget (e.g., Biddle & Swart, 2020) and sea ice interaction (e.g., Crews et al., 2022). The vertical resolution of our model may also result in limitations, as we do not fully resolve the very thin boundary layer at the ocean-sea ice interface where the surface fluxes are important. The number of vertical levels might be insufficient to fully resolve the dynamics on the very shallow Arctic shelves. These processes need to be further observed and investigated as they are likely contributing to the mixed layer salinity budget departing from its large scale 1-D balance.

Data Availability Statement

A full description of the simulation used in this study (CREG12.L75-REF08) as well as all the information required to produce the model output are available in open access at https://doi.org/10.5281/zenodo.5789520 and in Talandier and Lique (2021).

Acknowledgments
AS acknowledges the support of a CNES Postdoctoral fellowship. AS and NK were also supported by the European Space Agency's Climate Change Initiative (ESA CCI) under contract number 4000123663/18/I-NB, Phase 2 of the Sea_Surface_Salinity_CCI+R&D project, as specified in proposal reference ARG-003-130-OPT. CL and CT were supported by the project MEDLEY funded by JPI Climate and JPI Oceans, under the agreement ANR-19- JPOC-000. We also acknowledge funding from the CLIMArcTIC project funded by the "PPR Océan et Climat—France 2030" (contract ANR-22-POCE-0005). This work is a contribution to the TOSCA/SMOS-Ocean project supported by CNES. The pan-Arctic simulation was performed using HPC resources from the French GENCI-CINES center (Grant 2018-A0050107420).

References

Aksenov, Y., Karcher, M., Proshutinsky, A., Gerdes, R., De Cuevas, B., Golubeva, E., et al. (2016). Arctic pathways of Pacific water: Arctic Ocean Model Intercomparison experiments. *Journal of Geophysical Research: Oceans*, *121*(1), 27–59. https://doi.org/10.1002/2015JC011299

Allende, S., Treguier, A. M., Lique, C., de Boyer Montégut, C., Massonnet, F., Fichefet, T., & Barthélemy, A. (2024). Impact of ocean vertical-mixing parameterization on Arctic sea ice and upper-ocean properties using the NEMO-SI3 model. *Geoscientific Model Development*, *17*(20), 7445–7466. https://doi.org/10.5194/gmd-17-7445-2024

Årthun, M., Onarheim, I. H., Dörr, J., & Eldevik, T. (2021). The seasonal and regional transition to an ice-free Arctic. *Geophysical Research Letters*, *48*(1), e2020GL090825. https://doi.org/10.1029/2020gl090825

Barton, B. I., Lique, C., Lenn, Y. D., & Talandier, C. (2022). An ice-ocean model study of the mid-2000s regime change in the Barents Sea. *Journal of Geophysical Research: Oceans*, *127*(11), e2021JC018280. https://doi.org/10.1029/2021jc018280

Biddle, L. C., & Swart, S. (2020). The observed seasonal cycle of submesoscale processes in the Antarctic marginal ice zone. *Journal of Geophysical Research: Oceans*, *125*(6), e2019JC015587. https://doi.org/10.1029/2019JC015587

Blanke, B., & Delecluse, P. (1993). Variability of the Tropical Atlantic Ocean simulated by a general circulation model with two different mixed-layer physics. *Journal of Physical Oceanography*, *23*(7), 1363–1388. https://doi.org/10.1175/1520-0485(1993)023<1363:vottao>2.0.co;2

Brodeau, L., Barnier, B., Penduff, T., Treguier, A. M., & Gulev, S. (2010). ERA40-based atmospheric forcing for global ocean circulation models. *Ocean Modelling*, *31*(3), 88–104. https://doi.org/10.1016/j.ocemod.2009.10.005

Carmack, E. C. (2007). The alpha/beta ocean distinction: A perspective on freshwater fluxes, convection, nutrients and productivity in high-latitude seas. *Deep Sea Research Part II: Topical Studies in Oceanography*, *54*(23–26), 2578–2598. https://doi.org/10.1016/j.dsr2.2007.08.018

Crews, L., Lee, C. M., Rainville, L., & Thomson, J. (2022). Direct observations of the role of lateral advection of sea ice meltwater in the onset of autumn freeze up. *Journal of Geophysical Research: Oceans*, *127*(2), e2021JC017775. https://doi.org/10.1029/2021jc017775

Dewey, S. R., Morison, J. H., & Zhang, J. (2017). An edge-referenced surface fresh layer in the Beaufort Sea seasonal ice zone. *Journal of Physical Oceanography*, *47*(5), 1125–1144. https://doi.org/10.1175/jpo-d-16-0158.1

Dupont, F., Higginson, S., Bourdallé-Badie, R., Lu, Y., Roy, F., Smith, G., et al. (2015). A high-resolution ocean and sea-ice modelling system for the Arctic and North Atlantic oceans. *Geoscientific Model Development*, *8*(11), 1577–1594. https://doi.org/10.5194/gmd-8-1577-2015

Fofonoff, N. P., & Millard, R. C., Jr. (1983). Algorithms for computation of fundamental properties of seawater. In *Endorsed by Unesco/SCOR/ICES/IAPSO Joint Panel on Oceanographic Tables and Standards and SCOR Working Group 51*. Unesco Technical Papers in Marine Science, No. 44.

Haine, T. W., & Martin, T. (2017). The Arctic-Subarctic sea ice system is entering a seasonal regime: Implications for future Arctic amplification. *Scientific Reports*, *7*(1), 1–9. https://doi.org/10.1038/s41598-017-04573-0

Hu, X., Myers, P. G., & Lu, Y. (2019). Pacific water pathway in the Arctic Ocean and Beaufort Gyre in two simulations with different horizontal resolutions. *Journal of Geophysical Research: Oceans*, *124*(8), 6414–6432. https://doi.org/10.1029/2019JC015111

Hudson, P. A., Martin, A. C. H., Josey, S. A., Marzocchi, A., & Angeloudis, A. (2024). Drivers of Laptev Sea interannual variability in salinity and temperature. *Ocean Science*, *20*(2), 341–367. https://doi.org/10.5194/os-20-341-2024

Jackson, J. M., Williams, W. J., & Carmack, E. C. (2012). Winter sea-ice melt in the Canada Basin, Arctic Ocean. *Geophysical Research Letters*, *39*(3), L03603. https://doi.org/10.1029/2011gl050219

Janout, M., Hölemann, J., Juhls, B., Krumpen, T., Rabe, B., Bauch, D., et al. (2016). Episodic warming of near-bottom waters under the Arctic sea ice on the central Laptev Sea shelf. *Geophysical Research Letters*, *43*(1), 264–272. https://doi.org/10.1002/2015gl066565

Kacimi, S., & Kwok, R. (2022). Arctic snow depth, ice thickness, and volume from ICESat-2 and CryoSat-2: 2018–2021. *Geophysical Research Letters*, *49*(5), e2021GL097448. https://doi.org/10.1029/2021gl097448

Kawaguchi, Y., Kikuchi, T., & Inoue, R. (2014). Vertical heat transfer based on direct microstructure measurements in the ice-free Pacific-side Arctic Ocean: The role and impact of the Pacific water intrusion. *Journal of Oceanography*, *70*(4), 343–353. https://doi.org/10.1007/s10872-014-0234-8

Kinnard, C., Zdanowicz, C. M., Koerner, R. M., & Fisher, D. A. (2008). A changing Arctic seasonal ice zone: Observations from 1870–2003 and possible oceanographic consequences. *Geophysical Research Letters*, *35*(2), L02507. https://doi.org/10.1029/2007gl032507

Kolodziejczyk, N., & Gaillard, F. (2013). Variability of the heat and salt budget in the subtropical southeastern Pacific mixed layer between 2004 and 2010: Spice injection mechanism. *Journal of Physical Oceanography*, *43*(9), 1880–1898. https://doi.org/10.1175/jpo-d-13-04.1

Kwok, R. (2018). Arctic sea ice thickness, volume, and multiyear ice coverage: Losses and coupled variability (1958–2018). *Environmental Research Letters*, *13*(10), 105005. https://doi.org/10.1088/1748-9326/aae3ec

Lemke, P., & Manley, T. O. (1984). The seasonal variation of the mixed layer and the pycnocline under polar sea ice. *Journal of Geophysical Research*, *89*(C4), 6494–6504. https://doi.org/10.1029/jc089ic04p06494

Lind, S., Ingvaldsen, R. B., & Furevik, T. (2018). Arctic warming hotspot in the northern Barents Sea linked to declining sea-ice import. *Nature Climate Change*, *8*(7), 634–639. https://doi.org/10.1038/s41558-018-0205-y

Macdonald, R. W., Carmack, E. C., McLaughlin, F. A., Falkner, K. K., & Swift, J. H. (1999). Connections among ice, runoff and atmospheric forcing in the Beaufort Gyre. *Geophysical Research Letters*, *26*(15), 2223–2226. https://doi.org/10.1029/1999gl900508

Madec, G. & the NEMO System Team. (2016). Nemo ocean engine (Tech. Rep.No. 27). Institut Pierre-Simon Laplace (IPSL). https://doi.org/10.5281/zenodo.1464816

Manucharyan, G. E., & Thompson, A. F. (2017). Submesoscale sea ice-ocean interactions in marginal ice zones. *Journal of Geophysical Research: Oceans*, *122*(12), 9455–9475. https://doi.org/10.1002/2017jc012895

Meneghello, G., Marshall, J., Lique, C., Isachsen, P. E., Doddridge, E., Campin, J. M., et al. (2021). Genesis and decay of mesoscale baroclinic eddies in the seasonally ice-covered interior Arctic Ocean. *Journal of Physical Oceanography*, *51*(1), 115–129. https://doi.org/10.1175/jpo-d-20-0054.1

Moisan, J. R., & Niiler, P. P. (1998). The seasonal heat budget of the North Pacific: Net heat flux and heat storage rates (1950–1990). *Journal of Physical Oceanography*, *28*(3), 401–421. https://doi.org/10.1175/1520-0485(1998)028<0401:tshbot>2.0.co;2

Mulligan, R. P., & Perrie, W. (2019). Circulation and structure of the Mackenzie River plume in the coastal Arctic Ocean. *Continental Shelf Research*, *177*, 59–68. https://doi.org/10.1016/j.csr.2019.03.006

Oziel, L., Sirven, J., & Gascard, J. C. (2016). The Barents Sea frontal zones and water masses variability (1980–2011). *Ocean Science*, *12*(1), 169–184. https://doi.org/10.5194/os-12-169-2016

Pellichero, V., Sallée, J. B., Schmidtko, S., Roquet, F., & Charrassin, J. B. (2017). The ocean mixed layer under Southern Ocean sea-ice: Seasonal cycle and forcing. *Journal of Geophysical Research: Oceans*, *122*(2), 1608–1633. https://doi.org/10.1002/2016jc011970

Peralta-Ferriz, C., & Woodgate, R. A. (2015). Seasonal and interannual variability of pan-Arctic surface mixed layer properties from 1979 to 2012 from hydrographic data, and the dominance of stratification for multiyear mixed layer depth shoaling. *Progress in Oceanography*, *134*, 19–53. https://doi.org/10.1016/j.pocean.2014.12.005

Polyakov, I. V., Alkire, M. B., Bluhm, B. A., Brown, K. A., Carmack, E. C., Chierici, M., et al. (2020). Borealization of the Arctic Ocean in response to anomalous advection from sub-Arctic seas. *Frontiers in Marine Science*, *7*, 491. https://doi.org/10.3389/fmars.2020.00491

Regan, H., Lique, C., Talandier, C., & Meneghello, G. (2020). Response of total and eddy kinetic energy to the recent spinup of the Beaufort Gyre. *Journal of Physical Oceanography*, *50*(3), 575–594. https://doi.org/10.1175/jpo-d-19-0234.1

Ren, L., Speer, K., & Chassignet, E. P. (2011). The mixed layer salinity budget and sea ice in the Southern Ocean. *Journal of Geophysical Research*, *116*(C8), C08031. https://doi.org/10.1029/2010jc006634

Rousset, C., Vancoppenolle, M., Madec, G., Fichefet, T., Flavoni, S., Barthélemy, A., et al. (2015). The Louvain-La-Neuve sea ice model LIM3.6: Global and regional capabilities. *Geoscientific Model Development*, *8*(10), 2991–3005. https://doi.org/10.5194/gmd-8-2991-2015

Smith, M., Stammerjohn, S., Persson, O., Rainville, L., Liu, G., Perrie, W., et al. (2018). Episodic reversal of autumn ice advance caused by release of ocean heat in the Beaufort Sea. *Journal of Geophysical Research: Oceans*, *123*(5), 3164–3185. https://doi.org/10.1002/2018jc013764

Steele, M., Ermold, W., & Zhang, J. (2011). Modeling the formation and fate of the near-surface temperature maximum in the Canadian Basin of the Arctic Ocean. *Journal of Geophysical Research*, *116*(C11), C11015. https://doi.org/10.1029/2010jc006803

Stewart, K. D., & Haine, T. W. (2016). Thermobaricity in the transition zones between alpha and beta oceans. *Journal of Physical Oceanography*, *46*(6), 1805–1821. https://doi.org/10.1175/jpo-d-16-0017.1

Stroeve, J., & Notz, D. (2018). Changing state of Arctic sea ice across all seasons. *Environmental Research Letters*, *13*(10), 103001. https://doi.org/10.1088/1748-9326/aade56

Stroeve, J. C., Markus, T., Boisvert, L., Miller, J., & Barrett, A. (2014). Changes in Arctic melt season and implications for sea ice loss. *Geophysical Research Letters*, *41*(4), 1216–1225. https://doi.org/10.1002/2013gl058951

Talandier, C., & Lique, C. (2021). CREG12.L75-REF08. https://doi.org/10.5281/zenodo.5789520

Tarasenko, A., Supply, A., Kusse-Tiuz, N., Ivanov, V., Makhotin, M., Tournadre, J., et al. (2021). Properties of surface water masses in the Laptev and the East Siberian seas in summer 2018 from in situ and satellite data. *Ocean Science*, *17*(1), 221–247. https://doi.org/10.5194/os-17-221-2021

Timmermans, M. L. (2015). The impact of stored solar heat on Arctic sea ice growth. *Geophysical Research Letters*, *42*(15), 6399–6406. https://doi.org/10.1002/2015gl064541

Timmermans, M. L., Cole, S., & Toole, J. (2012). Horizontal density structure and restratification of the Arctic Ocean surface layer. *Journal of Physical Oceanography*, *42*(4), 659–668. https://doi.org/10.1175/jpo-d-11-0125.1

Toole, J. M., Timmermans, M. L., Perovich, D. K., Krishfield, R. A., Proshutinsky, A., & Richter-Menge, J. A. (2010). Influences of the ocean surface mixed layer and thermohaline stratification on Arctic Sea ice in the central Canada Basin. *Journal of Geophysical Research*, *115*(C10), C10018. https://doi.org/10.1029/2009jc005660

Treguier, A. M., Deshayes, J., Le Sommer, J., Lique, C., Madec, G., Penduff, T., et al. (2014). Meridional transport of salt in the global ocean from an eddy-resolving model. *Ocean Science*, *10*(2), 243–255. https://doi.org/10.5194/os-10-243-2014

Van Straaten, C., Lique, C., & Kolodziejcyk, N. (2025). The life cycle of the low salinity lenses at the surface of the Arctic Ocean. *Journal of Geophysical Research: Oceans*, *130*(4), e2024JC021699. https://doi.org/10.1029/2024jc021699

Woodgate, R. A. (2018). Increases in the Pacific inflow to the Arctic from 1990 to 2015, and insights into seasonal trends and driving mechanisms from year-round Bering Strait mooring data. *Progress in Oceanography*, *160*, 124–154. https://doi.org/10.1016/j.pocean.2017.12.007

Woodgate, R. A., Weingartner, T. J., & Lindsay, R. (2012). Observed increases in Bering Strait oceanic fluxes from the Pacific to the Arctic from 2001 to 2011 and their impacts on the Arctic Ocean water column. *Geophysical Research Letters*, *39*(24). https://doi.org/10.1029/2012GL054092